

## **AN ANALYSIS OF THE STEADY-STATE HEAT BALANCE METHOD FOR MEASURING SAP FLOW IN PLANTS**

J.M. BAKER<sup>1</sup> and J.L. NIEBER<sup>2</sup>

<sup>1</sup>*USDA-ARS, Department of Soil Science, University of Minnesota, St. Paul, MN 55108 (U.S.A.)*

<sup>2</sup>*Department of Agricultural Engineering, University of Minnesota, St. Paul, MN 55108 (U.S.A.)*

(Received July 26, 1988; revision accepted December 26, 1988)

### **ABSTRACT**

Baker, J.M. and Nieber, J.L., 1989. An analysis of the steady-state heat balance method for measuring sap flow in plants. *Agric. For. Meteorol.*, 48: 93-109.

An axisymmetric finite element model of heat flow was used to evaluate some of the assumptions inherent in the steady-state heat balance method for measuring sap flow in herbaceous plants. Results indicate that the gauge slightly overestimates conduction up and down the stem when sap flow is nearly zero, causing a corresponding underestimate of the sheath conductance and the radial outward heat flux. As sap flow rates increase, the temperature distribution in the stem and gauge is altered to the point that the one-dimensional Fourier equations are no longer applicable and the individual heat fluxes in the system are poorly estimated. However, the errors are largely self-compensating, so that the resulting gauge estimate of the heat absorbed by the sap stream is reasonably accurate. The model indicates that stem vascular anatomy affects the accuracy of the method, predicting that, in general, the method should be more accurate with dicots than with monocots.

### **INTRODUCTION**

Accurate measurement of plant water use has always been a difficult task for those interested in soil/plant/atmosphere relationships. A recent approach which has shown promise is the steady-state heat balance method developed by Sakuratani (1981, 1984). Use of this method does not alter any of the environmental or physiological factors affecting the transpiration process and Sakuratani reports an accuracy of  $\pm 10\%$ , a figure supported by the results of Baker and Van Bavel (1987), who worked with cotton and sunflowers in the laboratory, and Steinberg et al. (1988), who used young peach trees in a field and greenhouse study.

The method works in the following way. A steady, known amount of heat is

applied to a small segment of the stem from a thin flexible heater that encircles the stem and is itself encircled by foam insulation. In the steady state, this heat input to the segment must be balanced by heat fluxes out of the segment, of which there are four: conduction up the stem, conduction down the stem, conduction outward through the foam sheath and convection in the moving transpiration stream. The conductive fluxes are estimated by applying Fourier's Law, in the first two cases using the one-dimensional form and in the third case applying the integrated equation for radial flow in a semi-infinite cylinder.

The required thermal conductivities are known or can be measured; the required temperature gradients are estimated from the output of strategically placed thermocouples. One thermocouple is placed against the stem, just above the heater, with one junction 2 mm further up the stem than the other. The temperature difference across this differentially wired thermocouple, divided by the distance between them, is taken as the gradient in the upward, apical direction. The downward, basal gradient is obtained in the same manner from a similarly wired pair of thermojunctions placed against the stem below the heater. The radial outward gradient is obtained from a thermopile consisting of several thermojunctions in series on either side of a thin sheath surrounding the heater. Baker and Van Bavel (1987) or Sakuratani (1984) provide further details on the construction.

Subtraction of the conductive fluxes from the known heat input yields the heat transported by the moving sap. Dividing this residual heat by the product of the heat capacity of sap and the temperature difference between sap entering and leaving the heated segment directly yields the mass flow rate of the sap (eq. 1)

$$F = [P - LA (\Delta T_u/\Delta x + \Delta T_d/\Delta x) - K\Delta T_r] / (C_s (T_o - T_i)) \quad (1)$$

where  $F$  = sap flow rate ( $\text{g s}^{-1}$ );  $P$  = power to heater (W);  $L$  = stem thermal conductivity ( $\text{W m}^{-1} \text{ }^\circ\text{C}^{-1}$ );  $A$  = stem cross-sectional area ( $\text{m}^2$ );  $\Delta T_u/\Delta x$  = temperature gradient up the stem ( $^\circ\text{C m}^{-1}$ );  $\Delta T_d/\Delta x$  = temperature gradient down the stem ( $^\circ\text{C m}^{-1}$ );  $K$  = sheath conductance ( $\text{W }^\circ\text{C}^{-1}$ );  $\Delta T_r$  = temperature difference across thermopile ( $^\circ\text{C}$ );  $C_s$  = heat capacity of xylem sap ( $\text{J g}^{-1} \text{ }^\circ\text{C}^{-1}$ );  $T_o$  = temperature of sap leaving heated segment ( $^\circ\text{C}$ );  $T_i$  = temperature of sap entering heated segment ( $^\circ\text{C}$ ).

The method is direct, requires no calibration and requires no knowledge of the cross-sectional area of the xylem vessels. However, implicit in the derivation are a number of assumptions. Since these assumptions cannot be easily examined in a physical experiment, we used computer simulation to evaluate them, as has been done with other methods for measuring plant water use (Pickard and Puccia, 1972; Swanson and Whitfield, 1981). We examined the following questions.

- (i) Are heat fluxes in the system adequately estimated by the components

of eq. 1; i.e., are the temperature gradients measured on the surface of the stem representative of the gradients across the whole stem cross-section?

(ii) The sheath conductance used to calculate the radial outward flow of heat is typically calculated by difference, subtracting the measured upward and downward conductive fluxes from the known heat input during a period, typically near dawn, when sap flow is zero or nearly so (Sakuratani, 1984; Baker and Van Bavel, 1987). If some flow is occurring during this period, what is the effect on the calculated sheath conductance and what is the subsequent effect on measured sap flow rates?

(iii) How is the method affected by stem anatomy differences between monocotyledons, where vascular bundles are scattered throughout the stem cross-section and dicotyledons, where xylem elements are formed in an annular ring, with parenchyma tissue to the inside and epidermal tissue to the outside?

(iv) Is the accuracy of the method a function of the sap flow rate?

Questions relating to the design of the gauge, i.e., type and thickness of insulation used, placement of thermojunctions, etc., were not considered in this study.

#### MATERIALS AND METHODS

The gauge configuration upon which the model was based is described by Baker and Van Bavel (1987). The heater is a resin-coated Inconel foil of neg-

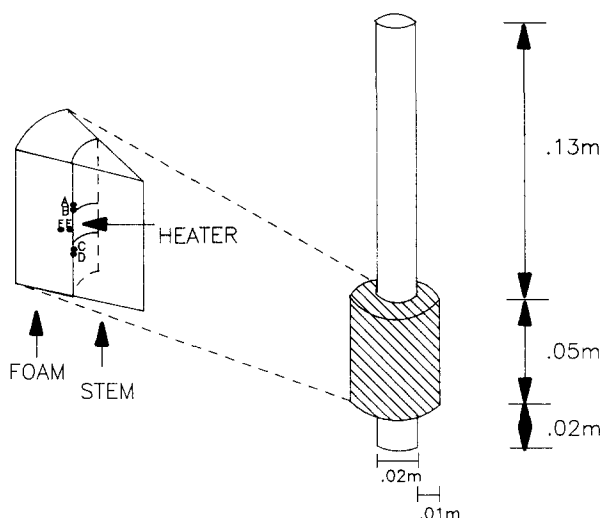


Fig. 1. Schematic of the stem-gauge system. Points A and B indicate the thermojunctions whose differential output is used to approximate the temperature gradient in the upward direction, while Points C and D indicate thermojunctions serving the same purpose for the downward direction. Points E and F represent two of the eight junctions forming a thermopile used to measure the radial outward temperature gradient. The change in sap temperature as it moves through the heated segment is obtained from the differential output across Junctions C and B.

ligible thickness and the insulation is a latex foam of 0.01-m thickness. The thermal conductivity of the foam was measured, using a line-source heating probe (Decagon Devices, Inc., Pullman, WA) as described by Jackson and Taylor (1986), while the thermal conductivity of the stem was taken as the mean of measured values for a range of herbaceous species reported by Sakuratani (1981).

Figure 1 illustrates the geometry of the modeled system. A stem radius of 0.01 m was used for both cases, with the insulation thickness also equal to 0.01 m. The length of the foam insulation was 0.05 m, extending equally in the basal and apical directions from the heater, which was 0.01 m wide. The total length of stem included in the model was 0.20 m. The lower boundary was assumed to be at the soil surface, 0.02 m below the lower edge of the foam insulation. The upper boundary was thus 0.13 m above the upper edge of the insulation.

## MATHEMATICAL ANALYSIS

### *Governing equations*

The heat transport problem, illustrated in Fig. 2(a), is three-dimensional, but due to the prevailing axisymmetric conditions, the problem can be reduced to one of axisymmetric heat conduction and convection. Also, for the present exercise sap flow and the temperature distribution in the stem are assumed to be at steady state. The governing partial differential equation for this problem is given by

$$\frac{1}{r} \left[ K_{rr} \frac{\partial}{\partial r} \left( r \frac{\partial T}{\partial r} \right) \right] + K_{zz} \frac{\partial^2 T}{\partial z^2} - FC_s \frac{\partial T}{\partial z} + Q = 0 \quad (2)$$

where  $K_{rr}$  and  $K_{zz}$  are the thermal conductivities in the radial and axial directions, respectively,  $T$  is the temperature,  $F$  is the rate of sap flow,  $C_s$  is the heat capacity of the sap and  $Q$  is a source/sink term. Sap flow is assumed to be in the axial direction only. The boundary conditions for the problem presented are listed below, in reference to Fig. 2(a).

$$T = T_a, z = 0 \quad 0 \leq r \leq r_s, 0 \leq \theta \leq 2\pi \quad (3a)$$

$$\frac{\partial T}{\partial z} = 0, z = z_t \quad 0 \leq r \leq r_s, 0 \leq \theta \leq 2\pi \quad (3b)$$

$$-K_{rr} \frac{\partial T}{\partial r} = h (T_s - T_a), \quad 0 \leq z \leq z_{fb}, z_{ft} \leq z \leq z_t, r = r_s, 0 \leq \theta \leq 2\pi \quad (3c)$$

$$-K_{rr} \frac{\partial T}{\partial r} = h (T_f - T_a), \quad z_{fb} \leq z \leq z_{ft}, r = r_f, 0 \leq \theta \leq 2\pi \quad (3d)$$

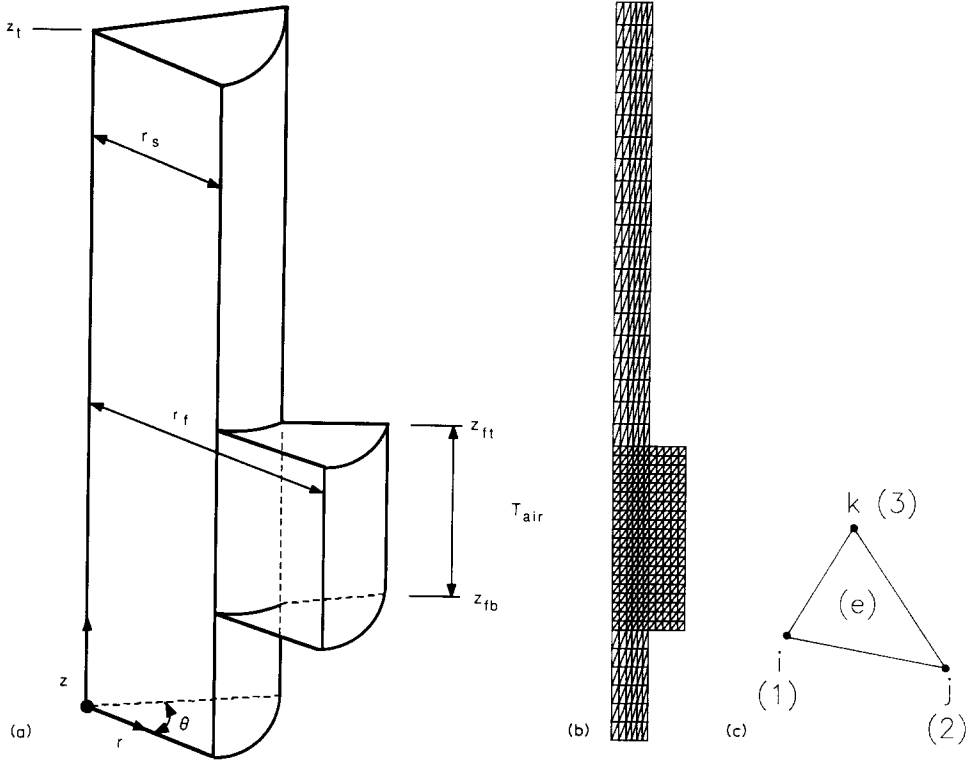


Fig. 2. (a) The domain of the heat flow problem. The applicable boundary conditions are described in the text. (b) The finite element grid imposed on the flow domain. (c) A single element of the grid.

where  $T_s$  and  $T_f$  are temperatures on the surface of the stem and foam, respectively, and  $T_a$  is the temperature of the surrounding air. In eq. 3c and d,  $h$  is a heat transfer coefficient, defined as

$$h = \rho C_a / r_a + \epsilon \sigma T_a^3 \quad (\text{J m}^{-2} \text{ s}^{-1} \text{ } ^\circ\text{C}^{-1})$$

where  $\rho$  and  $C_a$  are the density and heat capacity of air, respectively, and  $r_a$  is the aerodynamic resistance, calculated as a function of the ambient wind speed and the diameter of the stem in the manner described by Campbell (1977).  $\epsilon$  is the emissivity and  $\sigma$  is the Stefan Boltzmann constant ( $5.67 \times 10^{-8} \text{ W m}^{-2} \text{ K}^{-4}$ ). For the purposes of this analysis, wind speed was taken as  $2 \text{ m s}^{-1}$ , yielding an aerodynamic resistance of  $30 \text{ s m}^{-1}$ . The term  $\epsilon \sigma T_a^3$  is a radiative transfer coefficient, derived from the surface radiation balance,  $\epsilon \sigma T_s^4 - \epsilon \sigma T_a^4$ , by assuming equal emissivity for surface and surroundings, and writing  $T_s$  as  $T_a + dT$ . Expanding  $(T_a + dT)^4$  and dropping all terms cubic or greater in  $dT$  because of its small magnitude relative to  $T_a$  allows the radiation balance to be written as  $\epsilon \sigma T_a^3 (T_s - T_a)$ , which greatly simplifies solution (Campbell, 1977).

### Numerical solution

The finite element method was used to solve eq. 2, subject to the conditions given in eq. 3. The Galerkin formulation of the method of weighted residuals (Segerlind, 1984) was the specific procedure used to derive the finite element equations. This procedure yields the following set of linear algebraic equations for any given element such as the one shown in Fig. 2c

$$G_i^{(e)} = \sum_{j=1}^3 B_{ij}^{(e)} T_j^{(e)} + q_i^{(e)} + Q_i^{(e)} + f_{si}^{(e)} \quad i=1,2,3 \quad (4)$$

where

$(e)$  = refers to element  $e$

$G_i^{(e)}$  = residual equation for node  $i$  for element  $(e)$

$T_j^{(e)}$  = temperature at node  $j$

$$B_{ij}^{(e)} = \frac{\pi \bar{r}}{2A^{(e)}} (K_{rr} b_i b_j + K_{zz} c_i c_j) + \frac{FC_s \pi \bar{r} c_i}{3} + k_{ij}^{(e)}$$

$A^{(e)}$  = area of element  $(e)$

$Q_i^{(e)}$  = amount of the heat source located in the element which contributes to node  $i$

$\bar{r} = (r_1 + r_2 + r_3)/3$  = radial distance from the axis of the cylinder to the centroid of the element

$r_1, r_2, r_3$  = radial distances from the axis of the cylinder to nodes  $i, j$  and  $k$ , respectively, of the element

$b_i = z_i - z_{i+1}$

$c_i = r_{i+1} - r_i$

$$f_{si}^{(e)} = \frac{\pi h L_{i,i+1}}{3} (2r_i + r_{i+1}) + \frac{\pi h L_{i,i-1}}{3} (2r_i + r_{i-1})$$

$$q_i^{(e)} = (V_{i,i+1} L_{i,i+1} + V_{i,i-1} L_{i,i-1})/2$$

$V_{i,i+1}, V_{i,i-1}$  = rate of heat conduction across the two element sides connected to node  $i$

$$k_{ij}^{(e)} = \frac{\pi}{6} [hL_{i,i+1} (3r_i + r_{i+1}) + hL_{i,i-1} (3r_i + r_{i-1})] \text{ for } i=j$$

$$k_{ij}^{(e)} = \frac{\pi}{6} hL_{i,i+1} (r_i + r_j) \quad i \neq j$$

$$k_{ik}^{(e)} = \frac{\pi}{6} hL_{i,i-1} (r_i + r_k) \quad i \neq k$$

$L_{i,i+1}, L_{i,i-1}$  = length of the two element sides connected to node  $i$ .

In the above,  $i$  takes on the values 1, 2, 3 cyclically.

To obtain the global system of equations, the equations for individual elements are combined by matrix addition to yield:

$$G_i = \sum_{(e)} G_i^{(e)} = \sum_{j=1}^M B_{ij} T_j + q_i + Q_i + f_{si} = 0 \quad i=1,2,\dots,M \quad (5)$$

where  $M$  is the number of node points used to discretize the solution region. Here,  $q_i$  refers to the heat conduction across that portion of the solution region boundary connected to node  $i$ . For all nodes  $i$  on the interior of the solution region, the value of  $q_i$  is zero.

The boundary condition given by eq. 3a is implemented into eq. 5 by modifying the global stiffness matrix. The condition given by eq. 3b means that the boundary has no heat conduction. This condition is implemented by setting  $q_i$  to zero for nodes connected to element sides where eq. 3b applies. The conditions given by eq. 3c and d are already implemented into eqs. 4 and 5 through the  $k_{ij}^{(e)}$  and  $f_{si}^{(e)}$  terms. The implementation of these two conditions is outlined in the Appendix.

The finite element grid used in the analysis is illustrated in Fig. 2(b). The sap flow rate given by the term  $q$  in eq. 2 was assumed to be uniform in the  $z$  direction. Two distinct cases were simulated, one representing a monocot, for which the sap flow was assumed to be uniformly distributed in the radial dimension, and the other representing a typical dicot, for which sap flow was confined to an annular ring extending from 40 to 70% of the radius of the stem. This is a simplification of reality, but it is a recognition of a fundamental anatomical difference between monocots and dicots (Foster and Gifford, 1974).

The sap flow rate parameter was implemented into the finite element equations by assigning a non-zero value of  $F$  to elements where sap flow was assumed to occur. Heat fluxes of interest were calculated following solution of the temperature field, using finite difference forms of the appropriate differential equations (Carslaw and Jaeger, 1959). To compute the gauge estimate of sap flow under a given condition, the temperatures at points corresponding to the locations of the thermocouples were inserted in eq. 1. A range of sap flow rates from 0 to 100 g h<sup>-1</sup> was used. To put the flow rates in perspective, in a field with a stand density of 50 000 plants ha<sup>-1</sup>, a flow rate of 100 g per h per plant equals a field transpiration rate of 0.5 mm h<sup>-1</sup>, which is often equaled or exceeded on sunny summer days.

## RESULTS AND DISCUSSION

### *Determination of sheath conductance*

As stated earlier, sheath conductance is determined during a period of zero or near zero sap flow by measuring the conductive fluxes up and down the stem,

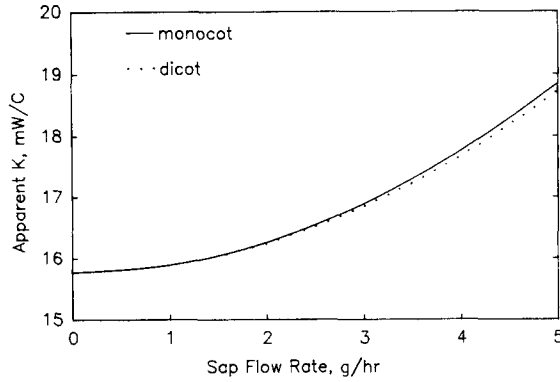


Fig. 3. Apparent sheath conductance. This conductance is calculated by difference during a period when sap flow is considered to be zero. The figure illustrates the effect on the calculated conductance if sap flow during the period was non-zero.

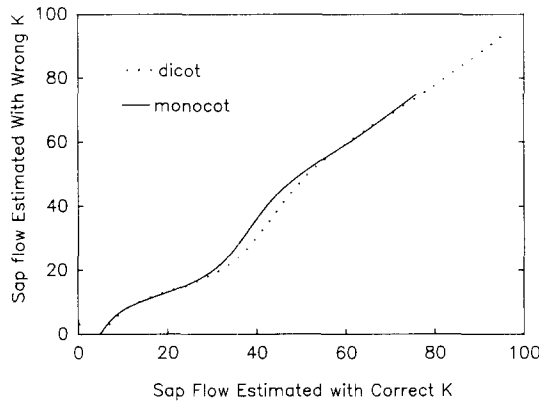


Fig. 4. The effect of using an incorrect sheath conductance. The figure shows sap flow estimated using a sheath conductance obtained during a period when sap flow was assumed to be zero, but was actually  $5 \text{ g h}^{-1}$ . It is plotted against sap flow estimated using a conductance obtained when sap flow was truly zero.

subtracting these from the heat input and dividing the result by the temperature difference across a thermopile surrounding the heated segment of stem. This was done with the model, with sap flow set to zero, and the sheath conductance obtained was then used in later simulations to obtain the apparent (gauge) sap flow rate at various true (model input) sap flow rates under various conditions. In a separate exercise, the sheath conductance was calculated for a range of input sap flow rates that were low, but non-zero.

Figure 3 shows the estimated sheath conductance as a function of sap flow rate for both the monocot and dicot. The results for the two are not greatly different. As expected, both converge to the “true” sheath conductance as sap

flow approaches zero and they both increase in exponential fashion as sap flow increases.

In practice, the sheath conductance has been determined in the field on intact plants in the pre-dawn hours (Sakuratani, 1984). However, even though transpiration may be negligible, there may still be sap flow associated with growth and/or rehydration. What is the consequence of using a value obtained under the assumption of zero flow if indeed flow was occurring? Figure 4 is a plot of gauge-estimated sap flow using an incorrect sheath conductance (obtained when flow was actually  $5 \text{ g h}^{-1}$  rather than zero) versus gauge-estimated sap flow using the true sheath conductance. Obviously, the error is greatest at low flow rates, but it diminishes in relative magnitude rapidly as sap flow increases, to the point of insignificance at flow rates  $> 50 \text{ g h}^{-1}$ .

### *Estimation of the heat fluxes*

To evaluate the assumptions about heat flow implicit in the heat balance method, the true conductive fluxes in the apical, basal and radial directions were computed element by element in the model and compared to the respective gauge estimates. The results, plotted against sap flow rate, are shown in Fig. 5 for the monocot model and Fig. 6 for the dicot. Considering first the situation in the absence of flow, the results indicate that the gauge overestimates both the apical and basal conductive fluxes by  $\sim 10\%$ . As a consequence, the radial heat flux is underestimated. As sap flow increases, the gauge continues to overestimate the apical heat flux and underestimate the radial heat flux. The basal heat flux, while overestimated at flow rates  $< 10 \text{ g h}^{-1}$ , is underestimated as sap flow increases beyond that point.

Isotherms for the respective systems help explain the results. Figure 7 shows the no-flow case. The inner rectangle delineates the volume for which the heat balance applies. The temperature gradients across the top and bottom boundaries of the control volume are steepest at the periphery of the stem, nearest the heater. Since the thermojunctions are located here, the gauge apparently overestimates the heat fluxes across these boundaries, in turn causing the underestimate of the radial heat flux.

Figure 8 shows the isotherms at a sap flow rate of  $100 \text{ g h}^{-1}$  for both the monocot and dicot. The temperature field is severely deformed at this flow rate, causing errors in estimates of heat fluxes based on assumptions of one-dimensional conduction which clearly do not apply. In the case of the monocot, the total conductive heat flux across the upper boundary is actually negative; i.e., the conductive heat flux is into the control volume rather than out of it, due to heat convected in the xylem sap near the surface of the stem that is then conducted inward and down the center of the stem.

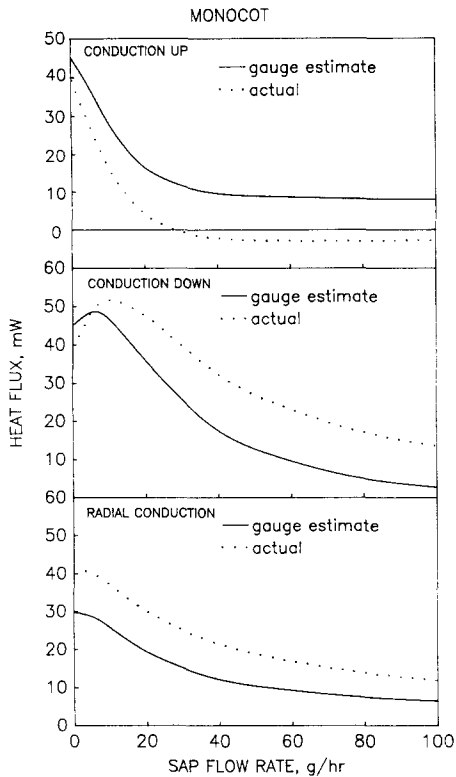


Fig. 5. Conductive fluxes in the stem-gauge system for the monocot.

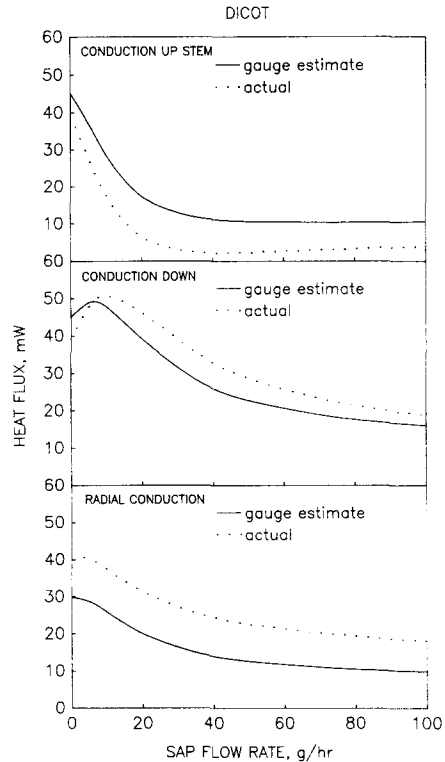


Fig. 6. Conductive fluxes in the stem-gauge system for the dicot.

### Overall accuracy

While estimates of the individual heat fluxes are of interest, the primary interest is in the overall accuracy in the estimation of the sap flow rate. To evaluate this, a range of sap flow rates was input to the model and the computed steady-state temperature differences were used in eq. 1, together with the previously determined (at zero flow) sheath conductance to obtain the gauge-estimated sap flow rate. Figure 9 shows the results for both the monocot and dicot. It indicates a noticeable difference between the two. For the dicot, the gauge result is very close to the 1:1 line. For the monocot, the gauge systematically underpredicts the sap flow rate, with the accuracy deteriorating as sap flow rate increases, so that at a true sap flow rate of  $100 \text{ g h}^{-1}$ , the gauge is in error by  $> 20\%$ .

In interpreting these results, the first step is to see how well the gauge predicts the residual heat, i.e., the heat absorbed by the transpiration stream. As Fig. 10 shows, for both simulations the gauge is reasonably close, meaning that

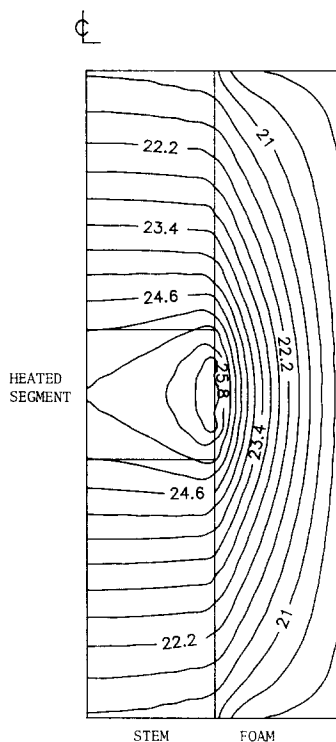


Fig. 7. Isotherms in the stem-gauge system in the absence of sap flow. The plot shows only the region including the gauge, with the smaller, inner rectangle delineating the region for which the measurement technique estimates the heat balance.

the underestimates of the basal and radial heat fluxes nearly balance the overestimate of the apical flux. From Fig. 10, it would appear that there is little difference in gauge performance between the monocot and the dicot, but this sap heat flux must be divided by the temperature difference between the sap entering and leaving the control volume in order to obtain the sap flow rate (eq. 1). The gauge estimates this from the difference in temperature between Points B and C (Fig. 1). The results indicate that this estimate is more accurate for the dicot than for the monocot and examination of the isotherms in Fig. 8 provides visual confirmation. It is important to note that this temperature difference ( $T_0 - T_i$  from eq. 1) decreases in magnitude as sap flow increases, so that thermocouple errors or bias due to conduction along the wires could affect the accuracy in a manner that this simulation would not address, since it was assumed that the gauge thermojunctions exactly measure the temperature at their locations.

A final point concerns the choice of the power input to the heater. The heat input used in the model was 0.12 W, uniformly distributed across the 0.01-m wide heater encircling the stem, but simulations with higher or lower levels of

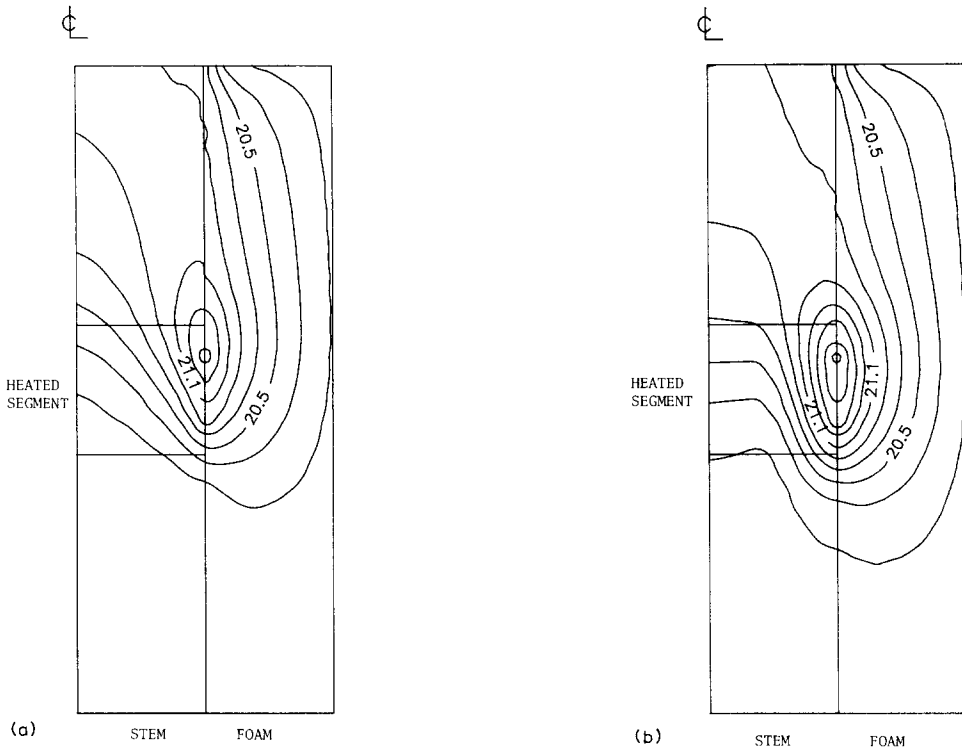


Fig. 8. Isotherms for the stem-gauge systems during steady sap flow of  $100 \text{ g h}^{-1}$ . The smaller rectangle delineates the region for which the heat balance is estimated. (a) monocot; (b) dicot.

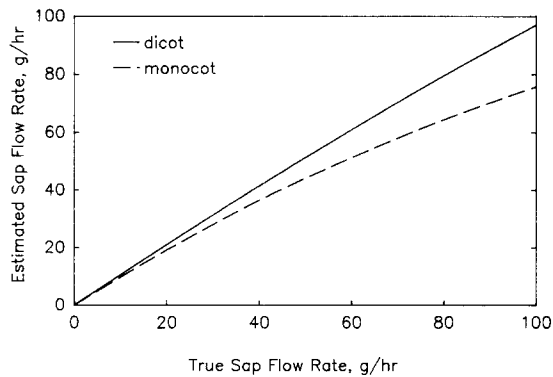


Fig. 9. Accuracy of the stem gauge in estimating sap flow rate. Gauge estimates of sap flow, as computed with the temperature distributions generated by the model, are plotted against the sap flow rates input to the model.

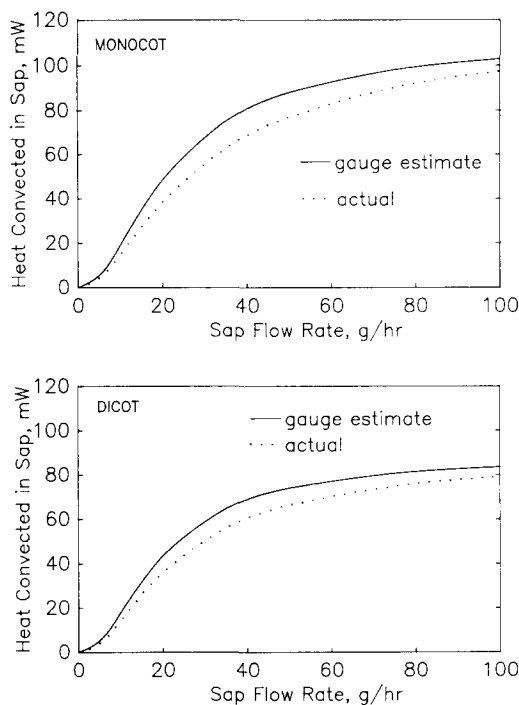


Fig. 10. Heat transported by convection out of the control volume. The gauge estimate is computed by difference, subtracting the estimated conductive fluxes from the known heat input. The “actual” is computed within the finite element model by multiplying the sap flux in each element on the boundary of the control volume by its temperature and the heat capacity of the sap.

heat input yield the same results since none of the transport coefficients are constrained by temperature dependence. In practical use of the method, the heat input level is determined by other considerations, i.e., it must be high enough to generate temperature differences resolvable by the data logger, but low enough to avoid physiological damage.

## CONCLUSIONS

Numerical solution of the governing equations has shown that stem anatomy affects the accuracy of the heat balance method for estimating sap flow rate. The method is predicted to be more accurate for dicotyledonous plants than for monocotyledonous plants, at least to the extent that their vascular structure conforms to the simplified assumptions made in this exercise. Assessment of the expected accuracy with a given species will require analysis with a model geometry tailored to match as closely as possible the stem anatomy of the species in question. A further crop-specific factor not considered was the effect of heterogeneity in thermal properties, which could be important

in species like soybean, which tend to develop voids in the center pith of the stem as they mature.

With respect to the sheath conductance, the model indicates both good news and bad. Because the gauge apparently overestimates apical and basal conduction in the zero sap flow condition, the sheath conductance will be underestimated to some extent. However, errors in the calculation of the sheath conductance, at least those associated with the presence of low flow rates during the supposed no-flow condition appear not to have serious consequences.

One cannot escape the conclusion that the overall success of the gauge in measuring transpiration is somewhat serendipitous, since the underlying assumptions about heat flow in the system lose much of their validity as sap flow increases. However, the errors in estimation of conduction tend to cancel one another, and the accuracy reported by users and confirmed by the simulation, at least for the case of the dicotyledon, is certainly sufficient to encourage further use of the method, especially since it is non-invasive and easy to use relative to alternative methods for measuring plant water use.

#### APPENDIX

The governing differential equations of steady state conductive and convective heat transfer in the stem of a plant is given by

$$L(T) = \frac{1}{r} \left[ K_{rr} \frac{\partial}{\partial r} \left( r \frac{\partial T}{\partial r} \right) \right] + K_{zz} \frac{\partial^2 T}{\partial z^2} - FC_s \frac{\partial T}{\partial z} + Q = 0 \quad (\text{A1})$$

where  $K_{rr}$  and  $K_{zz}$  are the thermal conductivities in the radial and axial coordinate directions,  $T$  is the temperature,  $F$  is the sap flow rate,  $C_s$  is the specific heat capacity of the sap and  $Q$  is a source/sink term.

The finite element solution of eq. A1 begins by assuming an approximate solution given by

$$T(r,z) \cong \tilde{T}(r,z) = [N] \{ \mathbf{T} \} \quad (\text{A2})$$

where  $[N]$  is a set of linearly independent interpolation (shape) functions and  $\{ \mathbf{T} \}$  is the vector of unknown temperatures at node points. The interpolation function defined by eq. A2 is usually defined over discrete elements, rather than over the entire solution region. Since eq. A2 is an approximate solution, substitution of this approximation into eq. A1 yields

$$L(\tilde{T}) = R(r,z) \neq 0$$

where  $R(r,z)$  is a residual error.

The method of weighted residuals (MWR) is used to eliminate this residual error in an average sense over the solution domain. In particular, the Galerkin procedure of the MWR is applied in the current analysis. This procedure is represented as

$$G_i = \int_{\Omega} N_i L(\tilde{T}) d\Omega = 0 \quad i=1,2,\dots,M$$

where  $N_i$  is the shape function for node  $i$  and  $M$  is the number of node points used to discretize the domain.

This integral statement indicates an integration over the entire solution domain, whereas it is usually advantageous to perform the integration on an element basis and then combine the results of individual elements to yield the result for the global domain. The integral statement for a discrete element is given by

$$G_i^{(e)} = \int_{\Omega^{(e)}} N_i L(\tilde{T}) d\Omega^{(e)} \quad i=1,2,\dots,p$$

where  $N_i$  is the shape function for mode  $i$  in element  $(e)$  and  $p$  is the number of node points in an element.

The second order derivatives in the integral statement must be reduced to first order because the second derivative of  $\tilde{T}$  will be undefined at element boundaries. The first derivatives are discontinuous at the element boundaries, but they constitute a finite discontinuity and the integral above is, therefore, defined. The reduction of the second order derivatives is accomplished using two-dimensional integration by parts to yield the following expression

$$G_i^{(e)} = \int_{\Gamma^{(e)}} N_i \left( K_{rr} \frac{\partial \tilde{T}}{\partial r} \cos \theta + K_{zz} \frac{\partial \tilde{T}}{\partial z} \sin \theta \right) d\Gamma^{(e)} - \int_{\Omega^{(e)}} \left( K_{rr} \frac{\partial N_i}{\partial r} \frac{\partial \tilde{T}}{\partial r} + K_{zz} \frac{\partial N_i}{\partial z} \frac{\partial \tilde{T}}{\partial z} \right) d\Omega^{(e)} + \int_{\Omega^{(e)}} N_i Q d\Omega^{(e)} - \int_{\Omega^{(e)}} N_i FC_s \frac{\partial \tilde{T}}{\partial z} d\Omega^{(e)} \quad (A3)$$

Substitution of the expression for  $\tilde{T}$  into eq. A3 yields

$$G_i^{(e)} = \int_{\Gamma^{(e)}} N_i \left( K_{rr} \frac{\partial \tilde{T}}{\partial r} \cos \theta + K_{zz} \frac{\partial \tilde{T}}{\partial z} \sin \theta \right) d\Gamma^{(e)} - \int_{\Omega^{(e)}} \left( K_{rr} \frac{\partial N_i}{\partial r} \frac{\partial [N]}{\partial r} + K_{zz} \frac{\partial N_i}{\partial z} \frac{\partial [N]}{\partial z} \right) d\Omega^{(e)} \{ \mathbf{T} \} + \int_{\Omega^{(e)}} N_i Q d\Omega^{(e)} - \int_{\Omega^{(e)}} N_i FC_s \frac{\partial [N]}{\partial z} d\Omega^{(e)} \{ \mathbf{T} \} \quad (A4)$$

For a linear triangular element, there are three node points and the terms in eq. A4 can be written as

$$G_i^{(e)} = \int_{\Gamma^{(e)}} N_i \left( K_{rr} \frac{\partial T}{\partial r} \cos \theta + K_{zz} \frac{\partial T}{\partial z} \sin \theta \right) d\Gamma^{(e)} - \sum_{j=1}^3 D_{ij}^{(e)} + Q_i^{(e)} \quad i=1,2,3 \quad (A5)$$

where

$$D_{ij}^{(e)} = \int_{\Omega^{(e)}} \left( K_{rr} \frac{\partial N_i}{\partial r} \frac{\partial N_j}{\partial r} + K_{zz} \frac{\partial N_i}{\partial z} \frac{\partial N_j}{\partial z} + N_i FC_s \frac{\partial N_i}{\partial z} \right) d\Omega^{(e)} = \left[ \frac{\pi \bar{r}}{2A} (K_{rr} b_i b_j + K_{zz} c_i c_j) + \frac{FC_s \pi \bar{r} c_i}{3} \right]^{(e)}$$

$$Q_i^{(e)} = \int_{\Omega^{(e)}} N_i Q d\Omega^{(e)} = \text{source strength at node } i$$

$b_i = z_i - z_{i+1}$ , where  $i$  takes on the values 1, 2, 3 cyclically

$c_i = r_{i+1} - r_i$ , where  $i$  takes on the values 1, 2, 3 cyclically.

Derivative boundary conditions for this problem are those of zero heat conduction given by

$$K_{rr} \frac{\partial T}{\partial r} \cos \theta + K_{zz} \frac{\partial T}{\partial z} \sin \theta = 0 \quad (\text{A6})$$

and convection given by

$$-\left( K_{rr} \frac{\partial T}{\partial r} \cos \theta + K_{zz} \frac{\partial T}{\partial z} \sin \theta \right) = h (T_s - T_a) \quad (\text{A7})$$

where  $T_s$  is the temperature at the element surface,  $T_a$  is the temperature of the surrounding air and  $h$  is the convection coefficient. Both of these conditions are implemented directly into eq. A5 through the first integral.

The substitution of eq. A6 produces a null result, but the substitution of eq. A7 produces non-zero terms. In the finite element formulation, the term  $h(T_s - T_a)$  is replaced by the approximation  $h([N] \{\mathbf{T}\} - T_a)$ . Substitution of eq. A7 with this approximation into eq. A5 yields for the first integral

$$-\int_{\Gamma^{(e)}} [N] h ([N] \{\mathbf{T}\} - T_a)^{(e)} d\Gamma^{(e)} = \frac{\pi h L_{i,j}}{6} \begin{bmatrix} (3r_i + r_j) & (r_i + r_j) & 0 & T_i \\ (r_i + r_j) & (r_i + 3r_j) & 0 & T_j \\ 0 & 0 & 0 & T_k \end{bmatrix} + \frac{\pi h L_{i,j}}{3} \begin{Bmatrix} 2r_i + r_j \\ r_i + r_j \\ 0 \end{Bmatrix} = [k]^{(e)} \{\mathbf{T}\}^{(e)} + \{f_s\}^{(e)}$$

for side  $i,j$  of the element. A similar element matrix form results for the  $j,k$  and  $k,i$  sides of the element. Note that the vector of unknown temperatures results from this substitution of the convection boundary condition. The coefficients in the  $[k]$  matrix are combined with the coefficient of the  $[D]$  matrix by matrix addition to yield for eq. A5,

$$G_i^{(e)} = q_i^{(e)} - \sum_{j=1}^3 B_{ij}^{(e)} T_j^{(e)} + Q_i^{(e)} + f_{si}^{(e)} \quad i=1,2,3$$

where

$$B_{ij}^{(e)} = D_{ij}^{(e)} + k_{ij}^{(e)}$$

$$q_i^{(e)} = (V_{i,i+1} L_{i,i+1} + V_{i,i-1} L_{i,i-1}) / 2$$

$V_{i,i+1}$ ,  $V_{i,i-1}$  = rate of heat conduction across the two sides of element ( $e$ ) connected to node  $i$ , and  $L_{i,i+1}$ ,  $L_{i,i-1}$  = length of the two sides of element ( $e$ ) connected to node  $i$

$$f_{si}^{(e)} = \frac{\pi h L_{i,i+1}}{3} (2r_i + r_{i+1}) + \frac{\pi h L_{i,i-1}}{3} (2r_i + r_{i-1})$$

In the above,  $i$  takes on the values 1, 2, 3 cyclically.

The global system of equations can be derived by adding the contributions from discrete elements into the global system of equations, i.e.

$$\begin{aligned} G_i = \sum_{(e)} G_i^{(e)} &= \sum_{j=1}^M (\sum_{(e)} B_{ij}^{(e)}) T_j - \sum_{(e)} q_i^{(e)} - \sum_{(e)} Q_i^{(e)} - \sum_{(e)} f_{si}^{(e)} \\ &= \sum_{j=1}^M B_{ij} T_j - q_i - Q_i - f_{si} = 0 \quad i=1,2,\dots, M \quad (A8) \end{aligned}$$

Note that  $q_i$  terms will be zero for all nodes on the interior and for insulated boundaries, and  $f_{si}$  terms will be zero for all nodes not on a boundary with convection.

## REFERENCES

- Baker, J.M. and Van Bavel, C.H.M., 1987. Measurement of mass flow of water in the stems of herbaceous plants. *Plant Cell Environ.*, 10: 777-782.
- Campbell, G.S., 1977. *An Introduction to Environmental Biophysics*. Springer Verlag, New York.
- Carslaw, H.S. and Jaeger, J.C., 1959. *Conduction of heat in solids*. Oxford University Press, London.
- Foster, A.S. and Gifford, E.M., 1974. *Comparative morphology of Vascular Plants*. Freeman, San Francisco, CA, 751 pp.
- Jackson, R.D. and Taylor, S.A., 1986. *Methods of Soil Analysis*. pp. 945-956. American Society of Agronomy, Madison, WI.
- Pickard, W.F. and Puccia, C.J., 1972. A theory of the steady-state heat step method of measuring water flux in woody plant stems. *Math Biosci.*, 14: 1-15.
- Sakurtani, T., 1981. A heat balance method for measuring water flux in the stem of intact plants. *J. Agric. Meteorol.*, 37: 9-17.
- Sakuratani, T., 1984. Improvement of the probe for measuring water flow rate in intact plants with the stem heat balance method. *J. Agric. Meteorol.*, 40: 273-277.
- Segerlind, L.J., 1984. *Applied Finite Element Analysis*. Wiley, New York, 427 pp.
- Steinberg, S., Van Bavel, C.H.M. and McFarland, M.J., 1989. Gauge to measure mass flow rate of sap in stems and trunks of woody plants. *Am. J. Hort. Sci.*, in press.
- Swanson, R.N. and Whitfield, D.W.A., 1981. Numerical analysis of heat pulse velocity theory. *J. Exp. Bot.*, 32: 221-239.